AIAA JOURNAL
Vol. 32, No. 10, October 1994

Bilinear Formulation Applied to the Response and Stability of Helicopter Rotor Blade

Grzegorz Kawiecki*
University of Tennessee, Knoxville, Tennessee 37996
and
Nithiam Ti Sivaneri†
West Virginia University, Morgantown, West Virginia 26506

A time finite element method based on Hamilton's law of varying action is applied to the analysis of helicopter blade dynamics. The bilinear formulation of Hamilton's law of varying action is used to discretize the temporal dependence of the equations of motion. Variable-order shape and test functions based on Legendre polynomials are used. Two approaches for the numerical implementation of the bilinear formulation are used. One approach obtains the response of a general dynamic system using marching in time. The other approach is based on the assumption that the solution is identical at the beginning and end of one period. Therefore, this approach is suitable for periodic systems. The bilinear formulation in imposed periodicity mode is used to compute the response of a rigid blade with flap and lag degrees of freedom in forward flight. The bilinear formulation in marching mode is applied to find the Floquet transition matrix necessary to test the stability of blade motion.

Nomenclature

$A(v)$ = linear operator on v
$B(q, v)$ = bilinear operator on q, v
C = damping matrix
C_D = drag coefficient
C_L = lift coefficient
c = blade chord, m
c_0, c_1 = coefficients in the expression for C_L
D = dissipation function
D_a = aerodynamic drag per unit length
d_0, d_1, d_2 = coefficients in the expression for C_D
E_L = matrix of Legendre polynomials
F = forcing function, N
G = test function matrix
H = shape function matrix
I = blade moment of inertia in Eq. (1), kg m^2, and identity matrix in Eq. (50)
K = stiffness matrix
L = Legendre polynomials
L_a = aerodynamic lift per unit length
L_{y_1} = aerodynamic load in the plane of rotation of the blade
L_{z_1} = aerodynamic load perpendicular to the plane of rotation of the blade
M = inertia matrix, generalized aerodynamic moments in Eqs. (1) and (2), Nm
ND = number of degrees of freedom
NS = number of shape functions
NT = number of time elements
P = generalized momentum, kgm/s
p = nodal displacement vector
q = displacement vector
$\tilde{q}$ = approximation to q
R = rotor radius
$\mathcal{R}$ = residuum
r = radial distance along elastic axis in Eq. (8), m, vector of arbitrary constants in Eqs. (21) and (23)
r_i = roots of Legendre polynomials
T = kinetic energy, Nm
U_P, U_T = blade cross section air velocity components, m/s
u = velocity, m/s
V = potential energy function, blade cross section resultant air velocity, m/s
v = vector of test functions
$\tilde{v}$ = vector of test function approximations
α = angle of attack, rad, $\theta - \phi_v$
β = blade flapping angle, rad
β_c = modified generalized coordinates
γ = Lock number, $3\rho acR/m$
ζ = blade lead-lag angle, rad
θ = blade pitch (obtained from trim solution)
Λ_k = kth eigenvalue of the transition matrix
λ = Lagrange multiplier
λ_i = induced velocity
λ_{in} = rotor inflow velocity
λ_k = real part of transition matrix kth eigenvalue complex exponent
μ = advance ratio
ν_β = dimensionless, rotating flapping natural frequency
Φ = transition matrix
ϕ_v = inflow angle at blade element, rad
Ψ = nondimensional time step length
ψ = nondimensional time, Ωt
Ω = rotor blade angular velocity, rad/s
ω_β = nondimensional, nonrotating flap frequency
ω_ζ = nondimensional, nonrotating lead-lag frequency

Introduction

MANY sophisticated aeroelastic models were recently developed to help in the design of advanced hingeless and bearingless helicopter rotors.[1–3] Those models make it easier to design rotors that take full advantage of the positive characteristics of advanced rotors, while minimizing the negative features inherent in the concept. Research in aeroelasticity of helicopter rotors has proven that the finite element method offers the most flexible approach in the spatial domain because of its capability to model complex blade-hub structures.[3] However, the accuracy of spatial aeroelastic models should be matched by the accuracy of mathe-

Received Sept. 5, 1991; revision received May 12, 1994; accepted for publication May 24, 1994.

*Assistant Professor, Department of Mechanical and Aerospace Engineering. Member AIAA.

†Professor, Department of Mechanical and Aerospace Engineering. Member AIAA.

matical methods used to obtain the solution in the temporal domain. One of the most promising methods that can be applied to the analysis of dynamic systems response and stability is the bilinear formulation of Hamilton's law of varying action.[4,5] The most important element of this method is the correct handling of the trailing terms in the numerical formulation of Hamilton's law of varying action. Very good convergence and stability of this approach in applications to linear dynamic systems have been reported. Previous studies[4,5] demonstrated the application of the bilinear formulation of Hamilton's law of varying action to analyze the dynamics of a single-degree-of-freedom linear dynamic system. The purpose of the present paper is to apply the bilinear formulation of Hamilton's law of varying action to the analysis of the dynamics of a helicopter rotor blade modeled as a multiple-degree-of-freedom, nonlinear, periodic system.

Formulation

The time finite element method based on Hamilton's law of varying action is applied to the analysis of the dynamics of a helicopter blade modeled as a two-degree-of-freedom rigid blade. The formulation of the differential equations of motion is outlined next.

Flap-Lag Equations of Motion

The feasibility of the imposed periodicity bilinear approach for the solution of nonlinear, multiple-degree-of-freedom rotary-wing dynamics problems is tested on a two-degree-of-freedom flap-lag blade model. This model is based on the rotor blade representation studied by Kaza and Kvaternik.[6] The geometry for aerodynamic velocity components is shown in Fig. 1.

The equations of motion are obtained using Lagrange's equations. The generalized aerodynamic moments M_β and M_ζ are evaluated using the principle of virtual work. The expressions for the kinetic energy T, the potential function V, and the dissipation function D are given in Ref. 6. The position vector of an arbitrary mass point coinciding with the elastic axis of the blade (with coordinates $x_1 = r$, $y_1 = 0$, and $z_1 = 0$) is obtained by the transformation from inertial axes $x\,y\,z$ fixed in the hub to the blade fixed axes $x_1\,y_1\,z_1$. A flap-lag transformation sequence is chosen for this system. The details of the transformation between the two coordinate systems and the details of the derivation of velocities U_T and U_P are given in Ref. 6. The equations of motion, with terms up to second order retained,[6] can be written as

$$I\ddot{\beta} + 2\Omega I\zeta\dot{\beta} + 2\zeta_\beta \nu_\beta \Omega I\dot{\beta} + \nu^2\Omega^2 I\beta = M_\beta$$
$$I\ddot{\zeta} - 2\Omega I\dot{\beta}\beta + 2\zeta_\zeta \omega_\zeta \Omega I\dot{\zeta} + \omega_\zeta^2\Omega^2 I\zeta = M_\zeta \tag{1}$$

where

$$M_\beta = (1/2)\rho c\cos(\zeta)\int_0^R r(C_L V U_T - C_D V U_P)\,dr$$
$$M_\zeta = -(1/2)\rho c\int_0^R r(C_L V U_P - C_D V U_T)\,dr \tag{2}$$

$$C_L = c_0 + c_1\alpha \tag{3}$$

$$C_D = d_0 + d_1\alpha + d_2\alpha^2 \tag{4}$$

$$\nu_\beta^2 = \omega_\beta^2 + 1 \tag{5}$$

$$\omega_\beta^2 = \frac{k_\beta}{\Omega^2 I} \tag{6}$$

$$\omega_\zeta^2 = \frac{k_\zeta}{\Omega^2 I} \tag{7}$$

Next, the equations of motion are nondimensionalized by dividing both sides by $I\Omega^2$. The nondimensionalized equations of motion can be written as

$$\ddot{\beta} + 2\dot{\zeta}\beta + 2\zeta_\beta\nu_\beta\dot{\beta} + (1+\omega_\beta^2)\beta = \frac{\gamma\cos(\zeta)}{2a}\int_0^1 r(C_L V U_T - C_D V U_P)\,dr$$
$$\ddot{\zeta} - 2\dot{\beta}\beta + 2\zeta_\zeta\omega_\zeta\dot{\zeta} + \omega_\zeta^2\zeta = -\frac{\gamma}{2a}\int_0^1 r(C_L V U_P - C_D V U_T)\,dr \tag{8}$$

Stability of Motion Analysis

The stability of motion is performed using Floquet's theorem. The stability analysis is based on Ref. 7. The eigenvalues Λ_k of the transition matrix are found and written in the exponential form. The real part λ_k of the complex characteristic exponent measures the stability of the response of the kth degree of freedom. Instability is indicated by $\lambda_k > 0$.

Discretization in Time

Marching-Mode Approach

The formulation presented here for the marching-mode approach is an extension of the formulation given in Ref. 8. Temporal discretization is achieved with the bilinear formulation of Hamilton's law of varying action. Consider the equation of motion

$$[M]\{\ddot{q}\} + [C]\{\dot{q}\} + [K]\{q\} = \{F\} \tag{9}$$

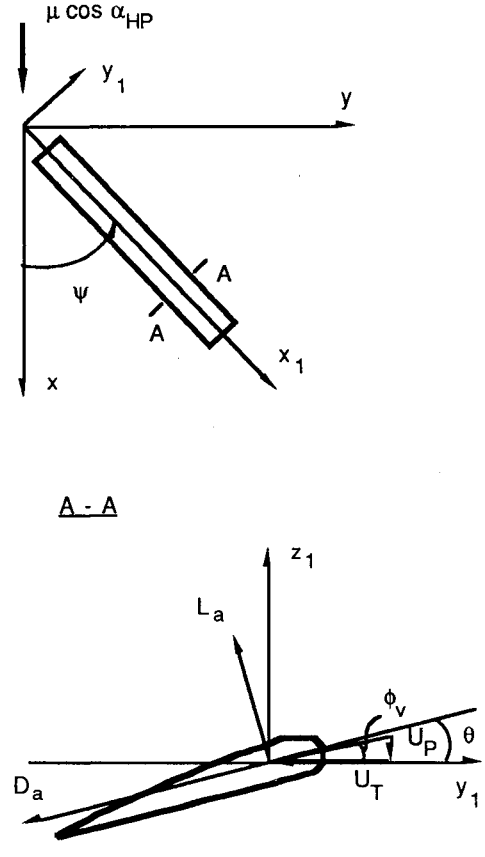

Fig. 1 Aerodynamic velocity components.

Multiplication by an arbitrary test function vector $\{v\}$ and integration over the domain $[0, \Psi]$ yields

$$\int_0^\Psi \{v\}^T ([M]\{\ddot{q}\} + [C]\{\dot{q}\} + [K]\{q\})\, d\psi = \int_0^\Psi \{v\}^T \{F\}\, d\psi \tag{10}$$

Rearrangement and integration by parts results in

$$\int_0^\Psi \begin{Bmatrix} \lfloor v \rfloor \\ \lfloor \dot{v} \rfloor \end{Bmatrix}^T \begin{Bmatrix} -[C]\{\dot{q}\} - [K]\{q\} \\ [M]\{\dot{q}\} \end{Bmatrix} d\psi = \begin{Bmatrix} \lfloor v \rfloor \\ \lfloor \dot{v} \rfloor \end{Bmatrix}^T \begin{bmatrix} \begin{Bmatrix} [M]\{\dot{q}\} \\ \{0\} \end{Bmatrix} \end{bmatrix}_0^\Psi - \int_0^\Psi \begin{Bmatrix} \lfloor v \rfloor \\ \lfloor \dot{v} \rfloor \end{Bmatrix}^T \begin{Bmatrix} \{F\} \\ \{0\} \end{Bmatrix} d\psi \tag{11}$$

The momenta at the beginning and end of the time period are defined as

$$[M]\{\dot{q}(0)\} = \{P_0\}$$
$$[M]\{\dot{q}(\Psi)\} = \{P_\Psi\} \tag{12}$$

Next, the definitions of the bilinear operator $B(q, v)$ and the linear operator $A(v)$ are introduced as

$$B(q, v) = \int_0^\Psi \begin{Bmatrix} \lfloor v \rfloor \\ \lfloor \dot{v} \rfloor \end{Bmatrix}^T \begin{Bmatrix} -[C]\{\dot{q}\} - [K]\{q\} \\ [M]\{\dot{q}\} \end{Bmatrix} d\psi \tag{13}$$

$$A(v) = \begin{bmatrix} \begin{Bmatrix} \lfloor v \rfloor \\ \lfloor \dot{v} \rfloor \end{Bmatrix}^T \begin{Bmatrix} \{P\} \\ \{0\} \end{Bmatrix} \end{bmatrix}_0^\Psi - \int_0^\Psi \begin{Bmatrix} \lfloor v \rfloor \\ \lfloor \dot{v} \rfloor \end{Bmatrix}^T \begin{Bmatrix} \{F\} \\ \{0\} \end{Bmatrix} d\psi \tag{14}$$

Then Eq. (11) is written, for all v, as

$$B(q, v) = A(v) \tag{15}$$

Integrating Eq. (13) by parts and rearranging Eqs. (13) and (15) yield

$$B(q, v) - \Big(A(v) = \int_0^\Psi \{v\}^T ([M]\{\ddot{q}\} + [C]\{\dot{q}\} + [K]\{q\}) - \{F\} \Big) d\psi + \{v(\Psi)\}^T \Big\{ \{P_\Psi\} - [M]\{\dot{q}(\Psi)\} \Big\} - \{v(0)\}^T \Big\{ \{P_0\} - [M]\{\dot{q}(0)\} \Big\} = 0 \tag{16}$$

The bilinear formulation of a dynamic problem[4,5] consists of Eq. (15) and Eqs. (13) and (14). Substitution of a trial function vector $\{\tilde{q}\}$ for the exact solution $\{q\}$ gives the error equation for numerical applications

$$\mathcal{R}(\tilde{q}, v) = B(\tilde{q}, v) - A(v) \tag{17}$$

For initial value problems with unknown $\{P_\Psi\}$, the test function vector $\{v(\Psi)\}$ should be chosen so that[4,5]

$$\{v(0)\} \neq \{0\} \quad \text{and} \quad \{v(\Psi)\} = \{0\} \tag{18}$$

This eliminates the unknowns from the error equation [Eq. (17)] and allows for automatic convergence of $\{P_0\} = [M]\{\dot{q}(0)\}$. Similarly, if $\{P_0\}$ is unknown, the test function vector should satisfy[4,5]

$$\{v(0)\} = \{0\} \quad \text{and} \quad \{v(\Psi)\} \neq \{0\} \tag{19}$$

Next, the displacement and test functions are discretized in the time domain

$$\{q\} = [H]\{p\} \tag{20}$$

$$\{v\} = [G]\{r\} \tag{21}$$

The present problem deals with an initial value problem. The displacement vector $\{q\}$ and the generalized momenta vector $\{P\}$ are known only at the initial point of the time element. Thus the constraints are[4,5]

$$\tilde{q}(0) = \{H(0)\}^T \{p\} = q_0 \tag{22}$$

$$\tilde{v}(\Psi) = \{G(\Psi)\}^T \{r\} = 0 \tag{23}$$

These constraints are included in Eq. (16) using a vector of Lagrange multipliers $\{\lambda\}$. The resulting system of equations can be written as

$$\begin{bmatrix} [B] & [G(\Psi)] \\ H(0) & [0] \end{bmatrix} \begin{Bmatrix} \{p\} \\ \{\lambda\} \end{Bmatrix} = \begin{Bmatrix} \{A\} \\ \{q_0\} \end{Bmatrix} \tag{24}$$

This allows the reduction of the size of $2N$ equations by N, where N is both the number of spatial degrees of freedom and the size of $\{\lambda\}$. The solution procedure can be done in three steps and is shown in the following text for a two-degree-of-freedom dynamic system modeled using the following matrix equation:

$$\begin{bmatrix} m_1 & 0 \\ 0 & m_2 \end{bmatrix} \begin{Bmatrix} \ddot{x}_1 \\ \ddot{x}_2 \end{Bmatrix} + \begin{bmatrix} c & -c \\ -c & c \end{bmatrix} \begin{Bmatrix} \dot{x}_1 \\ \dot{x}_2 \end{Bmatrix} + \begin{bmatrix} k_1 + k_2 & -k_2 \\ -k_2 & k_2 \end{bmatrix} \begin{Bmatrix} x_1 \\ x_2 \end{Bmatrix} = \begin{Bmatrix} F(t) \\ 0 \end{Bmatrix} \tag{25}$$

Assume that two nodes per time element are used, as shown in Fig. 2. Therefore, the components of Eq. (24) will have the following form:

$$[B] = \int_0^\Psi \left(\begin{bmatrix} G_1 & 0 & \dot{G}_1 & 0 \\ G_2 & 0 & \dot{G}_2 & 0 \\ 0 & G_1 & 0 & \dot{G}_1 \\ 0 & G_2 & 0 & \dot{G}_2 \end{bmatrix} \begin{bmatrix} c & -c \\ -c & c \end{bmatrix} \begin{bmatrix} \dot{H}_1 & \dot{H}_2 & 0 & 0 \\ 0 & 0 & \dot{H}_1 & \dot{H}_2 \end{bmatrix} \begin{bmatrix} -m_1 & 0 \\ 0 & -m_2 \end{bmatrix} \begin{bmatrix} \dot{H}_1 & \dot{H}_2 & 0 & 0 \\ 0 & 0 & \dot{H}_1 & \dot{H}_2 \end{bmatrix} + \begin{bmatrix} k_1 + k_2 & -k_2 \\ -k_2 & k_2 \end{bmatrix} \begin{bmatrix} H_1 & H_2 & 0 & 0 \\ 0 & 0 & H_1 & H_2 \end{bmatrix} \right) d\psi \tag{26}$$

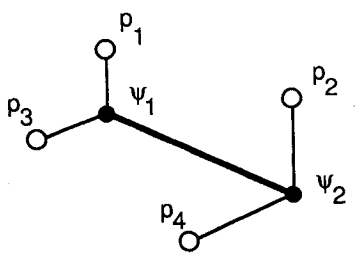

Fig. 2 Time element used for the marching-mode algorithm.

$$[G(\Psi)] = \begin{bmatrix} G_1(\Psi) & 0 \\ G_2(\Psi) & 0 \\ 0 & G_1(\Psi) \\ 0 & G_2(\Psi) \end{bmatrix} \tag{27}$$

where $G_1(\Psi) = 1$ and $G_2(\Psi) = 0$,

$$[H(0)] = \begin{bmatrix} H_1(0) & H_2(0) & 0 & 0 \\ 0 & 0 & H_1(0) & H_2(0) \end{bmatrix} \tag{28}$$

where $H_1(0) = 1$ and $H_2(0) = 0$, and

$$\{p\} = \begin{Bmatrix} p_1 \\ p_2 \\ p_3 \\ p_4 \end{Bmatrix} \tag{29}$$

$$\{\lambda\} = \begin{Bmatrix} \lambda_1 \\ \lambda_2 \end{Bmatrix} \tag{30}$$

$$\{A\} = \int_0^{\Psi} \begin{bmatrix} G_1(\psi) & 0 & \dot{G}_1(\psi) & 0 \\ G_2(\psi) & 0 & \dot{G}_2(\psi) & 0 \\ 0 & G_1(\psi) & 0 & \dot{G}_1(\psi) \\ 0 & G_2(\psi) & 0 & \dot{G}_2(\psi) \end{bmatrix} \begin{Bmatrix} F(\psi) \\ 0 \\ 0 \\ 0 \end{Bmatrix} d\psi + \begin{bmatrix} G_1(0) & 0 & \dot{G}_1(0) & 0 \\ G_2(0) & 0 & \dot{G}_2(0) & 0 \\ 0 & G_1(0) & 0 & \dot{G}_1(0) \\ 0 & G_2(0) & 0 & \dot{G}_2(0) \end{bmatrix} \begin{Bmatrix} m_1\dot{q}_1(0) \\ m_2\dot{q}_3(0) \\ 0 \\ 0 \end{Bmatrix} \tag{31}$$

Next, the approximations of the displacement vector and the velocity vector at the end of the time interval are computed. First, the unknown nodal displacements p_1 and p_2 are found

$$\begin{bmatrix} B_{22} & B_{24} \\ B_{42} & B_{44} \end{bmatrix} \begin{Bmatrix} p_2 \\ p_4 \end{Bmatrix} = \begin{Bmatrix} A_2 \\ A_4 \end{Bmatrix} - \begin{bmatrix} B_{21} & B_{23} \\ B_{41} & B_{43} \end{bmatrix} \begin{Bmatrix} p_1 \\ p_3 \end{Bmatrix} \tag{32}$$

Then, the vector of Lagrange multipliers λ is evaluated

$$\begin{Bmatrix} \lambda_1 \\ \lambda_2 \end{Bmatrix} = \begin{Bmatrix} A_1 \\ A_3 \end{Bmatrix} - \begin{bmatrix} B_{11} & B_{13} \\ B_{31} & B_{33} \end{bmatrix} \begin{Bmatrix} p_1 \\ p_3 \end{Bmatrix} - \begin{bmatrix} B_{12} & B_{14} \\ B_{32} & B_{34} \end{bmatrix} \begin{Bmatrix} p_2 \\ p_4 \end{Bmatrix} \tag{33}$$

Finally, the vector of velocities at the end of the time interval is determined

$$\begin{Bmatrix} \dot{p}_2(\Psi) \\ \dot{p}_4(\Psi) \end{Bmatrix} = \begin{bmatrix} m_1 & 0 \\ 0 & m_2 \end{bmatrix}^{-1} \begin{Bmatrix} \lambda_1 \\ \lambda_2 \end{Bmatrix} \tag{34}$$

For a nonlinear problem, with $[B]$ and $\{A\}$ dependent on $\{q\}$, Eq. (32) is solved for unknown nodal displacements p using a Levenberg-Marquardt algorithm and a finite difference approximation to the Jacobian. The initial guess for each time step is obtained by computing $[B(q)]$ and $\{A(q)\}$ with $\{q\}$ found for the preceding time step and solving the resulting linear system of equations.

Imposed-Periodicity Approach

The solution of a helicopter blade steady-state periodic-response problem can be largely facilitated by the assumption that the solution is identical at the beginning and end of one revolution. One can assemble the equations used in the marching mode and then impose the equality of the solution at the beginning and end of one period. The process of assembly is shown next for a one-degree-of-freedom periodic system modeled using the following equation:

$$m\ddot{x}(\psi) + c(\psi)\dot{x}(\psi) + k(\psi)x(\psi) = F(\psi) \tag{35}$$

where the forcing function $F(\Psi)$ as well as the damping coefficient $c(\Psi)$ and the stiffness coefficient $k(\Psi)$ are periodic, whereas the inertia matrix m is constant.

The time interval of length equal to one period is divided for two time elements as shown in Fig. 3. It is assumed that the initial nodal displacement for the first time element p_1^1 is equal to the final nodal displacement for the second time element p_2^2. Similarly, the equivalence of the velocity u_1^1 at the beginning of the first time element and the velocity u_2^2 at the end of the second time element is imposed. Linear basis functions are used in each time element. The bilinear formulation gives rise to the following system of equations for the first time element:

$$\begin{bmatrix} [B] & \begin{Bmatrix} G_1(\Psi) \\ G_2(\Psi) \end{Bmatrix} \\ \lfloor H_1(0), H_2(0) \rfloor & 0 \end{bmatrix} \begin{Bmatrix} p_1^1 \\ p_2^1 \\ \lambda \end{Bmatrix} = \begin{Bmatrix} \int_0^{\Psi} \begin{bmatrix} G_1 & \dot{G}_1 \\ G_2 & \dot{G}_2 \end{bmatrix} \begin{Bmatrix} F \\ 0 \end{Bmatrix} d\psi + \begin{bmatrix} G_1(0) & \dot{G}_1(0) \\ G_2(0) & \dot{G}_2(0) \end{bmatrix} \begin{Bmatrix} [M]\{u_1^1\} \\ 0 \end{Bmatrix} \\ p_1^1 \end{Bmatrix} \tag{36}$$

where

$$[B] = \int_0^{\Psi} \begin{bmatrix} G_1 & \dot{G}_1 \\ G_2 & \dot{G}_2 \end{bmatrix} \begin{Bmatrix} [C]\lfloor \dot{H}_1, \dot{H}_2 \rfloor + [K]\lfloor H_1, H_2 \rfloor \\ -[M]\lfloor \dot{H}_1, \dot{H}_2 \rfloor \end{Bmatrix} d\psi \tag{37}$$

Therefore

$$\begin{bmatrix} B_{11} & B_{12} & 1 \\ B_{21} & B_{22} & 0 \\ 1 & 0 & 0 \end{bmatrix} \begin{Bmatrix} p_1^1 \\ p_2^1 \\ \lambda \end{Bmatrix} = \begin{Bmatrix} \int_0^{\Psi} \begin{Bmatrix} G_1 \\ G_2 \end{Bmatrix} \lfloor F \rfloor d\psi + \begin{Bmatrix} G_1(0) \\ G_2(0) \end{Bmatrix} [M]\{u_1^1\} \\ p_1^1 \end{Bmatrix} \tag{38}$$

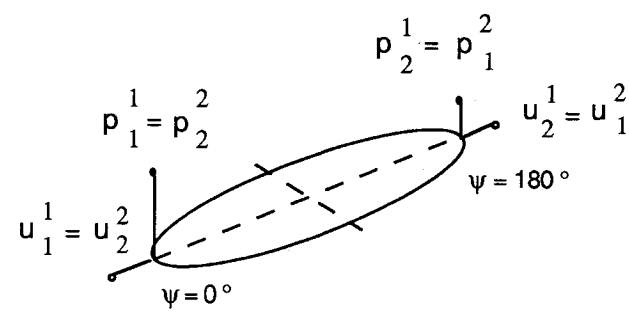

Fig. 3 Nodal displacements and velocities for the imposed-periodicity algorithm.

where p_1^1 is known, p_2^1 is unknown, u_1^1 is known, and λ is unknown.

The term p_2^1 is determined using the following equation:

$$B_{22}^1 p_2^1 = \int_0^{\Psi} G_2(\psi) F \, d\psi + G_2(0) M u_1^1 - B_{21}^1 p_1^1 \tag{39}$$

λ and u_2^1 are determined using

$$\lambda = \int_0^{\Psi} G_1(\psi) F \, d\psi + G_1(0) M u_1^1 - B_{11}^1 p_1^1 - B_{12}^1 p_2^1 \tag{40}$$

and

$$u_2^1 = M^{-1}\lambda \tag{41}$$

Therefore, the system of equations for element 1 can be written in matrix form as

$$\begin{bmatrix} B_{21}^1 & 0 \\ B_{12}^1 & M \end{bmatrix} \begin{Bmatrix} p_2^1 \\ u_2^1 \end{Bmatrix} = \begin{Bmatrix} \int_0^{\Psi} G_2(\psi) F \, d\psi + G_2(0) M u_1^1 - B_{21}^1 p_1^1 \\ \int_0^{\Psi} G_1(\psi) F \, d\psi + G_1(0) M u_1^1 - B_{11}^1 p_1^1 - B_{12}^1 p_2^1 \end{Bmatrix} \tag{42}$$

Finally, remembering that $u_2^2 = u_1^1$ and $p_2^2 = p_1^1$, we can write the final system of equations:

$$\begin{bmatrix} B_{22}^1 & 0 & B_{21}^1 & -G_2(0) M \\ B_{12}^1 & M & B_{11}^1 & -G_1(0) M \\ B_{21}^2 & -G_2(0) M & B_{22}^2 & 0 \\ B_{11}^2 & -G_1(0) M & B_{12}^2 & M \end{bmatrix} \begin{Bmatrix} p_2^1 \\ u_2^1 \\ p_2^2 \\ u_2^2 \end{Bmatrix} = \begin{Bmatrix} \int_0^{\Psi} G_2(\psi) F \, d\psi \\ \int_0^{\Psi} G_1(\psi) F \, d\psi \\ \int_0^{\Psi} G_2(\psi) F \, d\psi \\ \int_0^{\Psi} G_1(\psi) F \, d\psi \end{Bmatrix} \tag{43}$$

In the same manner one can assemble a system of N equations over N time elements. Certain elements in the upper right corner of the coefficient matrix are nonzero due to the imposition of periodicity. This destroys the bandedness of the matrix. The number of shape functions can be arbitrary. The solution procedure for nonlinear problems, with $[B]$ and $\{F\}$ dependent on $\{q\}$, is similar to that used for the marching-mode approach. Equation (43) is solved for unknown nodal displacements p and end-node velocities u using a Levenberg-Marquardt algorithm and a finite difference approximation to the Jacobian. The initial guess is obtained by neglecting the nonlinear terms in Eq. (43) and solving the resulting linear system of equations.

Basis Functions

The basis functions used in this study are based on the Legendre polynomials. The Legendre polynomials were selected over ordinary power series for two reasons:

1) The coefficient matrix constructed with ordinary power series is poorly conditioned. Therefore, the inverse of this matrix is less accurate, and convergence problems may be encountered.[9]

2) Recursive formulas for calculating the values of the Nth-order Legendre polynomials and their derivatives at a given point are readily available. Application of the power series to equally spaced internal nodes gives rise to shape functions in terms of the Lagrange polynomials. An extensive literature search did not reveal a recursive formula for the Lagrange polynomial derivatives.

This development is based on Ref. 10. Displacement $q(\tau)$ is written in terms of a set of Legendre polynomials:

$$q(\tau) = \{L(\tau)\}^T \{\alpha_c\} \tag{44}$$

where $\{L(\tau)\}^T$ is the vector of Legendre polynomial values, and $\{\alpha_c\}$ is the vector of generalized coordinates.

For an approximation based on the Legendre polynomials, the n internal nodes are roots r_i of a Legendre polynomial of order n over the interval $[-1, 1]$. However, the set of nodes for a time interval should contain the endpoints to preserve the displacement continuity at the ends of the time interval. Therefore, the modified shape functions $\{H\}$ will be spanned over the following set of nodes:

$$\tau_1 = -1$$

$$\tau_2 = r_1$$

$$\vdots$$

$$\tau_{n-1} = r_{n-2}$$

$$\tau_n = 1$$

Then the displacement can be written in terms of modified shape functions:

$$q(\tau) = \lfloor H(\tau) \rfloor \{\beta_c\} \tag{45}$$

where

$$\{\beta_c\} = \begin{bmatrix} \lfloor L(-1) \rfloor \\ \lfloor L(r_1) \rfloor \\ \vdots \\ \lfloor L(1) \rfloor \end{bmatrix} \{\alpha_c\} = [E_L]\{\alpha_c\} \tag{46}$$

Equations (39) and (41) give rise to a system of equations that allows us to calculate the vector of modified shape-function values at $\tau \in [-1, 1]$:

$$[E_L]^T \{H(\tau)\} = \{L(\tau)\} \tag{47}$$

Similarly, we can calculate the vector of shape-function derivatives at τ:

$$[E_L]^T \{H'(\tau)\} = \{L'(\tau)\} \tag{48}$$

The recurrence formulas used to calculate the value and the derivative of the Legendre polynomial of order n for a given coordinate $\tau \in [-1, 1]$ are presented in Ref. 11.

Results and Discussion

Convergence Study for One-Degree-of-Freedom Rigid-Blade Model

A series of numerical experiments is conducted with both the marching-mode approach and the imposed-periodicity approach. The goal of these experiments is to determine the convergence characteristics of both methods and to investigate the influence on the overall result of the number of time elements NT per revolution and the order of basis functions NS approximating the spatial solution over one time element. The number of basis functions NS per time element was equal to the number of time nodes per time element. This study is conducted on the example of a simple rigid flapping response problem, described by the following equation:

$$\ddot{\beta} + \frac{\gamma}{8}\left[1 + \frac{4}{3}\mu \sin(\psi)\right]\dot{\beta} + \left[1 + \frac{\gamma}{8}\left(\frac{4}{3}\mu \cos(\psi) + \mu^2 \sin(2\psi)\right)\right]\beta = F \tag{49}$$

Table 1 Convergence study for the marching-mode approach

Number of time elements	Number of shape functions per time element	CPU time, s	Displacement error, %	Velocity error, %
2	2	1.14	1.13888E + 04	1.95898E + 02
2	4	1.25	3.43373E + 01	2.08087E + 00
2	8	1.54	3.46445E − 04	3.60966E − 06
2	12	2.09	5.27296E − 09	3.39932E − 10
2	16	3.32	6.43891E − 11	4.62843E − 12
4	2	1.15	6.96566E + 02	4.03847E + 01
4	4	1.29	4.24280E − 02	2.85189E − 02
4	8	1.78	5.90300E − 08	4.93699E − 12
4	12	2.63	1.82916E − 10	1.05058E − 11
4	16	4.62	4.55435E − 11	8.81606E − 14
6	2	1.23	2.14053E + 02	1.89087E + 01
6	4	1.49	3.54271E − 03	1.97476E − 03
6	8	1.97	2.86503E − 11	1.09760E − 11
6	12	3.12	9.56498E − 11	7.37611E − 12
6	16	5.74	1.73856E − 09	5.44979E − 11
8	2	1.23	1.02186E + 02	1.07938E + 01
8	4	1.53	2.72465E − 04	3.51199E − 04
8	8	2.24	4.86653E − 10	2.61690E − 11
8	12	4.00	6.73899E − 10	3.78356E − 11
8	16	6.77	9.82262E − 10	5.83329E − 11

Table 2 Convergence study for the imposed-periodicity approach

Number of time elements	Number of shape functions per time element	CPU time, s	Displacement error, %	Velocity error, %
2	2	0.89	1.09828E + 04	1.83560E + 02
2	4	0.88	3.43373E + 01	2.08087E + 00
2	8	1.03	3.46444E − 04	3.60968E − 06
2	12	1.58	5.53417E − 09	3.31719E − 10
2	16	3.07	1.99088E − 10	5.70105E − 12
4	2	0.86	6.96565E + 02	4.03848E + 01
4	4	0.87	4.24280E − 02	2.85189E − 02
4	8	1.16	5.92744E − 08	1.83374E − 11
4	12	2.04	1.91766E − 10	4.30517E − 12
4	16	4.27	3.16321E − 10	1.16519E − 11
6	2	0.85	2.14053E + 02	1.89087E + 01
6	4	0.94	3.54271E − 03	1.97476E − 03
6	8	1.31	2.92870E − 10	8.22833E − 13
6	12	2.54	2.37649E − 10	7.09693E − 12
6	16	5.73	2.09203E − 09	7.24239E − 11
8	2	0.90	1.02186E + 02	1.07938E + 01
8	4	0.95	2.72464E − 04	3.51199E − 04
8	8	1.47	1.09253E − 10	2.15993E − 12
8	12	3.19	2.70480E − 10	1.79113E − 11
8	16	7.45	9.71609E − 10	4.57994E − 11

where

$$F = \frac{\gamma}{8}\left[\theta\left(1 + \frac{8}{3}\mu\sin(\psi) + 2\mu^2\sin^2(\psi)\right) + \frac{4}{3}\lambda_{in} - 1.46\sqrt{\nu_\beta}\lambda_i\cos(\psi) + 2\mu\lambda_{in}\sin(\psi)\right]$$

The details of the derivation are given in Ref. 12, p. 153. The following values are used:

$$\gamma = 5.00 \qquad \mu = 0.20 \qquad \lambda_i = 0.04$$

$$\theta = 0.20 \qquad \lambda_{in} = -0.03 \qquad \nu_\beta = 1.15$$

An ordinary differential equation with periodic coefficients has a unique periodic solution if the determinant of $([I] - [\Phi(2\pi, 0)]) \neq 0$ (Ref. 7). The value of $\det([I] - [\Phi(2\pi, 0)])$ computed for Eq. (49) is equal 0.754002004861831665. Therefore, this equation has a unique periodic solution. The following initial condition must be used to obtain the unique periodic solution of Eq. (49) (Ref. 7):

$$\{y(0)\} = \left([I] - [\Phi(2\pi, 0)]\right)^{-1} \int_0^{2\pi} [\Phi(2\pi, s)]\{F(s)\}\, ds \qquad (50)$$

The initial condition given by Eq. (50) is found using the method outlined in Ref. 7. Then, Eq. (50) is integrated numerically using a fifth-order Runge-Kutta-Verner method with the small step ($\Delta\psi = 1$ deg) and very low global error ($\varepsilon = 10^{-13}$). The converged solution is regarded to be the exact periodic solution of Eq. (49). Then, the program based on the marching-mode approach is run with the following initial conditions: $\beta(0) = 0$ and $\dot{\beta}(0) = 0$. The program is run until the differences between two consecutive values of $\dot{\beta}(2\pi)$ cease to decrease. The values of $\beta(2\pi)$ and $\dot{\beta}(2\pi)$ obtained in this way are compared with the Runge-Kutta solution. The runs are made for one revolution, divided into 2, 4, 6, and 8 time elements and for 2, 4, 8, 12, and 16 shape functions per time element. The results are shown in Table 1. Similar tests are performed for the imposed-periodicity approach. However, that approach does not require any initial conditions. The results are shown in Table 2. Tables 1 and 2 also give the CPU times for each run. Table 1 shows good convergence characteristics of the marching-mode bilinear approach. The slight increase in error that occurs for $NT > 2$ and $NS \geq 8$ can be explained by roundoff error. The smallest displacement error for the marching mode occurs for $NT = 6$ and $NS = 12$. Also, the closer the method is to the h-version finite element method, the faster the solution is obtained. This is confirmed by the comparison of CPU time for three cases shown in Table 1. The number of nodes for each of these cases is equal to 32. The cases are characterized by the following combinations of number of time elements NT and number of shape functions NS:

1) $NT = 2$ and $NS = 16$.
2) $NT = 4$ and $NS = 8$.
3) $NT = 8$ and $NS = 4$.

Of these, the fastest was the solution for $NT = 8$ and $NS = 4$, and the slowest was the solution for $NT = 2$ and $NS = 16$. The latter was also most accurate in terms of displacement error. This observation gives an important insight into the accuracy vs computational time for the marching-mode approach. The analysis of the results given in Table 2 indicates good convergence too. The slight increase of error for $NT > 2$ and $NS \geq 8$ can be explained as before, i.e., with roundoff error. The observations regarding the number of time elements vs the number of basis functions that were made for the marching-mode bilinear approach also can be made for the imposed-periodicity bilinear approach.

It is interesting to compare the performance of both approaches. The imposed-periodicity approach is consistently less accurate than the marching-mode approach. However, the imposed-periodicity approach is generally faster than the marching-mode approach, with the exception of one case where the combination of $NT = 8$ and $NS = 16$ results in the largest system of equations. The speed advantage of the imposed-periodicity approach decreases with the increase of the size of the system of equations. It is necessary to point out that the difference in CPU time depends significantly on the initial conditions used in the marching-mode approach.

Another aspect is the memory requirement for both methods. In the case of the marching approach, the memory requirement depends on the number of degrees of freedom ND for the system and the number of shape functions NS. In the case of the imposed-periodicity approach, the memory requirement depends also on the number of time elements NT. The marching-mode bilinear solver has to solve in each step a system of algebraic equations of size $(NS - 1) \cdot ND$ to calculate the displacement vector. After the displacement vector is found, a separate system of equations of the order $ND \cdot ND$ is solved for the velocity at the end of the time element. This procedure has to be repeated NT times.

The imposed-periodicity bilinear solver solves a system of algebraic equations of size $NS \cdot ND \cdot NT$. For periodic systems with many degrees of freedom this may lead to very large systems of equations.

Stability Analysis for One-Degree-of-Freedom Rigid-Blade Model

The stability analysis is based on Eq. (49), with $F = 0$, and uses Floquet theory to determine the stability boundaries. The numerical analysis is performed using the marching-mode bilinear formulation algorithm modified to calculate λ_k values for an arbitrary system of linear differential equations. The results are correlated with those of Ref. 13, and the agreement is very good. The variation of $Re\ \lambda_k$ with μ for $\gamma = 11.2$ computed using the marching-mode bilinear formulation is compared in Fig. 4 with data shown in Fig. IV-1, p. 59, and in Fig. IV-A, p. 62, of Ref. 13. The stability limit occurs for $\mu \approx 1.41$, which is again in good agreement with Ref. 13.

Response Analysis for Two-Degree-of-Freedom Rigid-Blade Model

The parameters corresponding to the steady-state forward flight β_0, β_{1c}, $\beta 1s$, θ_0, θ_{1c}, θ_{1s}, λ, α_{HP}, and ϕ_s are obtained by solving a system of nine algebraic equations constituting the helicopter propulsive trim problem. This system of equations consists of three

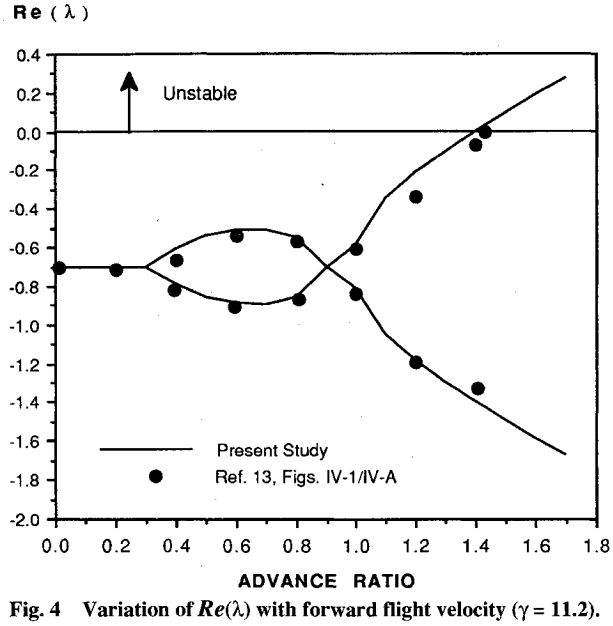

Fig. 4 Variation of $Re(\lambda)$ with forward flight velocity ($\gamma = 11.2$).

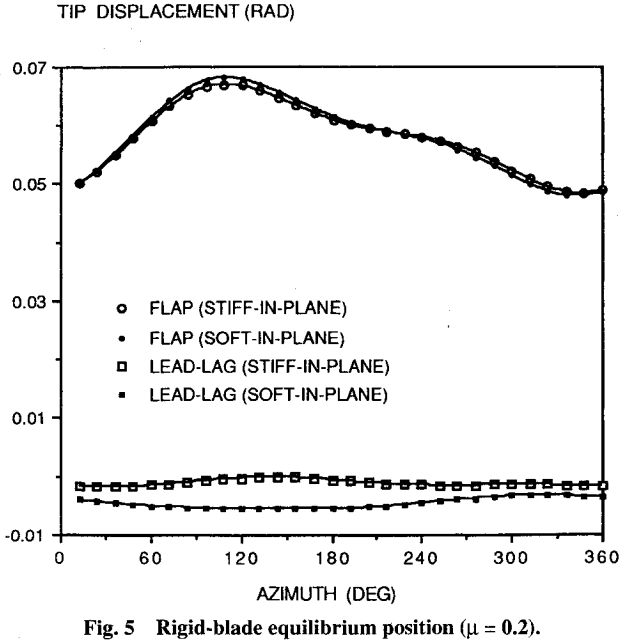

Fig. 5 Rigid-blade equilibrium position ($\mu = 0.2$).

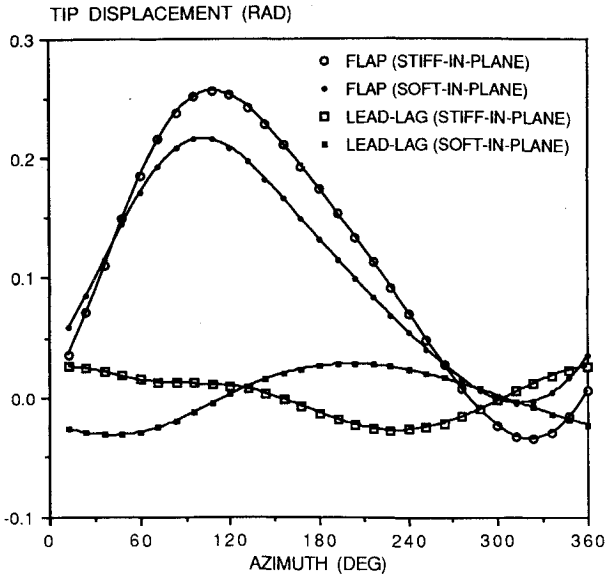

Fig. 6 Rigid-blade equilibrium position ($\mu = 0.4$).

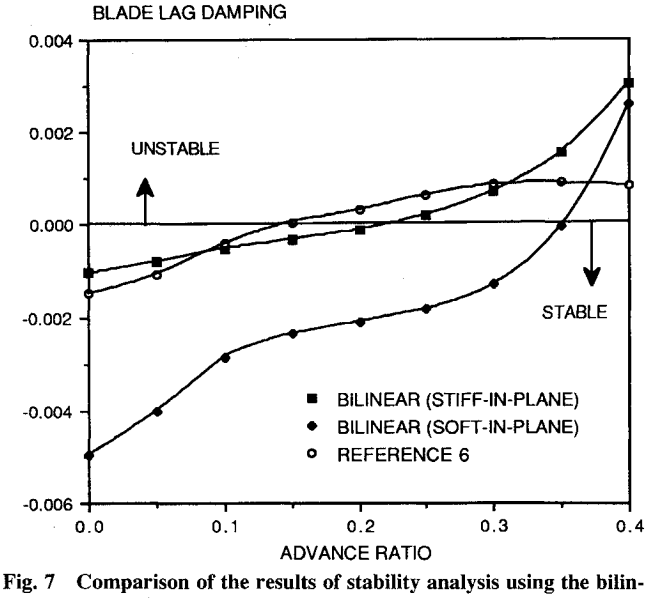

Fig. 7 Comparison of the results of stability analysis using the bilinear approach with the results presented in Ref. 6.

equations of equilibrium of forces, two equations of equilibrium of moments (about pitch and roll axes), three rotor equilibrium equations, and an induced flow equation.

The trim algorithm is based on Ref. 14 and was validated by reproducing the trim results (not shown here) presented in that reference. The response of the blade represented by the two-degree-of-freedom, flap-lag model is investigated for four values of advance ratio μ and two values of rotating lag frequencies ν_ζ. The values of ν_ζ are selected to match rotating lag frequencies for soft in-plane rotors ($\nu_\zeta = 0.7$) and stiff in-plane rotors ($\nu_\zeta = 1.4$). The results were compared with those of Ref. 14. A quantitative comparison was not possible because the assumptions regarding the induced flow and the number of degrees of freedom considered in both models were different. Qualitatively, the trends and the amplitudes determined by both studies were similar. Example time histories of the response over one revolution are shown in Figs. 5 and 6. These steady-state solutions are used in the stability analysis of flap-lag blade motion to validate the results obtained using the bilinear formulation against the results of stability analysis presented in Ref. 6. They are obtained for the following blade and aerodynamic properties:

$$\beta_p = 0.0 \qquad c_0 = 0.0$$

$$C_T/\sigma = 0.1 \qquad c_1 = 5.7$$

$\gamma = 5.0$ $\quad d_0 = 0.01$

$\alpha = 5.7$ $\quad d_1 = 0.0$

$C_{mac} = 0.0$ $\quad \nu_\beta = 1.15$

Stability Analysis for Two-Degrees-of-Freedom, Flap-Lag Rigid-Blade Model

Equations (8) are perturbed and linearized about the blade nonlinear steady-state position. The steady-state position for given flight parameters is determined using the imposed-periodicity approach. The Floquet transition matrix for the linearized system is computed using the marching-mode bilinear formulation algorithm, as in the case of one-degree-of-freedom rigid-blade-model stability analysis. Then the values of λ_k indicating the stability characteristics of the system are determined. The results for the stiff in-plane rotor are correlated with Ref. 6, and the agreement is good. The comparison is presented in Fig. 7. The differences in the two solutions can be attributed to the different trim procedures and to a different method used to obtain the nonlinear blade equilibrium position in Ref. 6. More important may seem the difference in the trends of the solutions. However, the trend of the result obtained using the bilinear formulation is in agreement with the newer stability results for stiff in-plane rotors presented in Refs. 15–17. Figure 7 also shows the results of stability analysis for a soft in-plane rotor. It is clear that the soft in-plane rotor is more stable than the stiff in-plane rotor. This trend is also demonstrated in Refs. 14–16.

The previous results show the feasibility of applying the bilinear formulation to the dynamic system stability analysis. The approach shown here represents the *h-p* version of the time finite element method, in the sense that one can change both the number of finite elements in the finite element model and the number of approximation functions per element. This method allows us to divide one revolution into smaller time elements and to choose an appropriate balance between the number of time elements and the order of basis functions for each element.

Conclusions

The conclusions of this study are the following:

1) The bilinear formulation of Hamilton's law of varying action can be used to solve nonlinear helicopter rotor dynamics problems.

2) The numerical implementation of the bilinear formulation is slightly less accurate in the imposed-periodicity mode than in the marching mode, and it imposes more severe computer memory requirements. However, the imposed-periodicity algorithm does not require initial conditions to solve linear periodic systems.

3) The speed advantage of the numerical implementation of the bilinear formulation in the imposed-periodicity mode over its implementation in the marching mode decreases with the increase of the resulting system of equations size.

4) Both implementations of the bilinear formulation show an increase in speed and a decrease in accuracy when the balance between the number of time elements and the number of shape functions shifts from $-p$ method to $-h$ method.

5) The bilinear formulation in the imposed-periodicity mode introduced in this paper is a promising and convenient-to-use tool, both for linear and nonlinear systems, but needs further improvements, e.g., incorporating a sparse equations solver to improve the numerical efficiency.

Acknowledgments

This research was partially supported by National Science Foundation Grant MSM-8504942. Financial support provided by Du Pont Washington Works, Parkersburg, WV, in the years 1988–1990 is gratefully acknowledged.

References

[1]Straub, F. K., and Friedmann, P. P., "A Galerkin Type Finite Element Method for Rotary Wing Aeroelasticity in Hover and Forward Flight," *Vertica*, Vol. 5, 1981, pp. 75–98.

[2]Sivaneri, N. T., and Chopra, I., "Dynamic Stability of a Rotor Blade Using Finite Element Analysis," *AIAA Journal*, Vol. 20, No. 5, 1982, pp. 716–723.

[3]Sivaneri, N. T., and Chopra, I., "Finite Element Analysis for Bearingless Rotor Blade Aeroelasticity," *Journal of The American Helicopter Society*, Vol. 29, No. 2, 1984, pp. 42–51.

[4]Izadpanah, A., "*p*-Version Finite Elements for the Space-Time Domain with Application to Floquet Theory," Ph.D. Thesis, Aerospace Engineering Dept., Georgia Inst. of Technology, Atlanta, GA, Aug. 1986.

[5]Peters, D. A., and Izadpanah, A. P., "*hp*-Version Finite Elements for the Space-Time Domain," *Computational Mechanics*, Vol. 3, 1988, pp. 73–88.

[6]Kaza, K. R. V., and Kvaternik, R. G., "Examination of the Flap-Lag Stability of Rigid Articulated Blades," *Journal of Aircraft*, Vol. 16, No. 12, 1979, pp. 876–884.

[7]Friedmann, P. P., "Numerical Methods for Determining the Stability and Response of Periodic Systems with Applications to Helicopter Rotor Dynamics and Aeroelasticity," *Computers & Mathematics with Applications*, Vol. 12A, No. 1, 1986, pp. 131–148.

[8]Sivaneri, N. T., and Kawiecki, G., "Forward Flight Aeroelasticity of a Hingeless Rotor Blade by Bilinear Formulation," AIAA/ASME/ASCE/AHS/ASC 30th Structures, Structural Dynamics, and Materials Conference, AIAA Paper 89-1233, Mobile, AL, April 1989.

[9]Hitzl, D. L., "Implementing Hamilton's Law of Varying Action with Shifted Legendre Polynomials," *Journal of Computational Physics*, Vol. 38, 1980, pp. 185–211.

[10]Hodges, D. H., and Rutkowski, M., "Free Vibration Analysis of Rotating Beams by a Variable-Order Finite Element Method," *AIAA Journal*, Vol. 19, No. 11, 1981, pp. 1459–1466.

[11]Andrews, L. C., *Special Functions for Engineers and Applied Mathematicians*, Macmillan, New York, 1985.

[12]Bramwell, A. R. S., *Helicopter Dynamics*, Wiley, New York, 1976, p. 153.

[13]Hall, W. E., "Application of Floquet Theory to the Analysis of Rotary Wing VTOL Stability," Ph.D. Dissertation, Dept. of Aeronautics and Astronautics, Stanford Univ., Stanford, CA, Feb. 1970, pp. 59–62.

[14]Panda, B., and Chopra, I., "Flap-Lag-Torsion Stability in Forward Flight," *Journal of The American Helicopter Society*, Vol. 30, Oct. 1985, pp. 30–39.

[15]Friedmann, P. P., and Kottapalli, S. B. R., "Coupled Flap-Lag-Torsional Dynamics of Hingeless Rotor Blades in Forward Flight," *Journal of the American Helicopter Society*, Vol. 27, No. 4, 1982, pp. 28–36.

[16]Gaonkar, G. H., and Peters, D. A., "Use of Multiblade Coordinates for Helicopter Flap-Lag Stability with Dynamic Inflow," *Journal of Aircraft*, Vol. 17, No. 2, 1980, pp. 112–118.

[17]Peters, D. A., and Gaonkar, G. H., "Theoretical Flap-Lag Damping with Various Dynamic Inflow Models," *Journal of the American Helicopter Society*, Vol. 25, No. 3, 1980, pp. 29–36.